The EMBO Journal vol.6 no.6 pp.1565–1570, 1987

# The molecular structure of insecticyanin from the tobacco hornworm *Manduca sexta* L. at 2.6 Å resolution



**Hazel M.Holden, Wojciech R.Rypniewski , John H.Law and Ivan Rayment**

Department of Biochemistry, Biological Sciences West, University of Arizona, Tucson, AZ 85721, USA

Communicated by R.Henderson

**Insecticyanin, a blue biliprotein isolated from the tobacco hornworm *Manduca sexta* L., is involved in insect camouflage. Its three-dimensional structure has now been solved to 2.6 Å resolution using the techniques of multiple isomorphous replacement, non-crystallographic symmetry averaging about a local 2-fold rotation axis and solvent flattening. All 189 amino acids have been fitted to the electron density map. The map clearly shows that insecticyanin is a tetramer with one of its molecular 2-fold axes coincident to a crystallographic dyad. The individual subunits have overall dimensions of 44 Å × 37 Å × 40 Å and consist primarily of an eight-stranded anti-parallel β-barrel flanked on one side by a 4.5-turn α-helix. Interestingly the overall three-dimensional fold of the insecticyanin subunit shows remarkable similarity to the structural motifs of bovine β-lactoglobulin and the human serum retinol-binding protein. The electron density attributable to the chromophore is unambiguous and shows that it is indeed the γ-isomer of biliverdin. The biliverdin lies towards the open end of the β-barrel with its two propionate side chains pointing towards the solvent and it adopts a rather folded conformation, much like a heme.**

*Key words:* bile pigment/biliprotein/insecticyanin/protein crystallography

## Introduction

Insecticyanin is a blue biliprotein found in the hemolymph and integument of the tobacco hornworm *Manduca sexta* L. and, in conjunction with the yellow carotenoids, plays an integral role in the camouflage coloration of the insect (Kawooya *et al.*, 1985). The protein was first isolated and purified by Cherbas (1973) and results from his work led to the proposal that biliverdin IXγ is the chromophore responsible for giving insecticyanin its intense blue coloration. The chromophore is tightly bound to the protein and can only be removed under denaturing conditions such as treatment with formamide (Cherbas, 1973) or guanidine hydrochloride (Riley *et al.*, 1984).

Since the original work of Cherbas, an improved purification scheme has been developed and the amino acid sequence determined (Riley *et al.*, 1984). Each 'apo'-subunit contains 189 amino acid residues and two disulfide bridges. There is, however, some discrepancy in the literature as to the quaternary structure of insecticyanin. One study concludes that the protein is a trimer (Goodman *et al.*, 1985) whereas the studies of Riley *et al.* (1984) suggest that insecticyanin, in solution, is a tetramer.

One of the interesting aspects of insecticyanin is the remarkable stability of the holoprotein during the radical restructuring that accompanies insect metamorphosis. Indeed, insecticyanin is produced only during the larval life stage of the insect but persists throughout the pupal stage and into the adult female hemolymph from which it is ultimately sequestered into the egg (Cherbas, 1972; Riddiford, 1982).

We initiated an X-ray crystallographic study of insecticyanin in light of both its central role in the cryptic coloration of the insect and its extraordinary stability during insect metamorphosis (Holden *et al.*, 1986). In this paper we describe the X-ray crystallographic determination of the insecticyanin structure to 2.6 Å resolution.

## Results

A portion of the insecticyanin electron density map, calculated at 2.6 Å resolution, is shown in Figure 1. The map is of sufficient quality to allow complete chain tracing starting from the N-terminal glycine and ending with the C-terminal histidine. Both the N-terminal and C-terminal regions are well ordered, salt bridges are clearly visible and there are numerous small peaks, particularly near oxygen and nitrogen atoms, that most likely correspond to ordered water molecules. The backbone density is weak in only three regions, all of which contain a glycine residue. Two of these 'breaks' occur between amino acid residues 52–54 and 95–98 and are located in β-turns at the surface of the molecule. The third break, between residues 141 and 143, occurs in the loop leading to the major helix and is also at the molecular

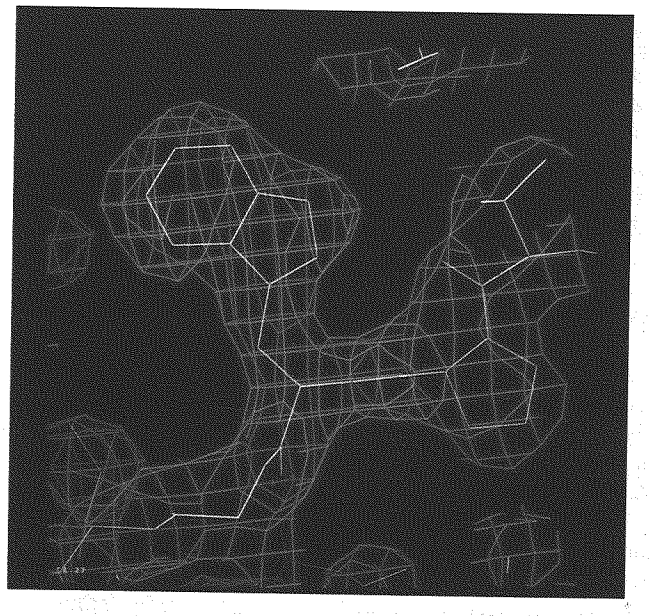

**Fig. 1.** Representative portion of the insecticyanin electron density map. The electron density map shown here has been solvent flattened and averaged about a local 2-fold rotation axis. Amino acid side chains shown correspond to Trp 104 and Pro 103. The quality of the electron density displayed here is consistent throughout the entire protein map. The photograph was taken from an Evans and Sutherland PS330 graphics system using the molecular modeling program FRODO.

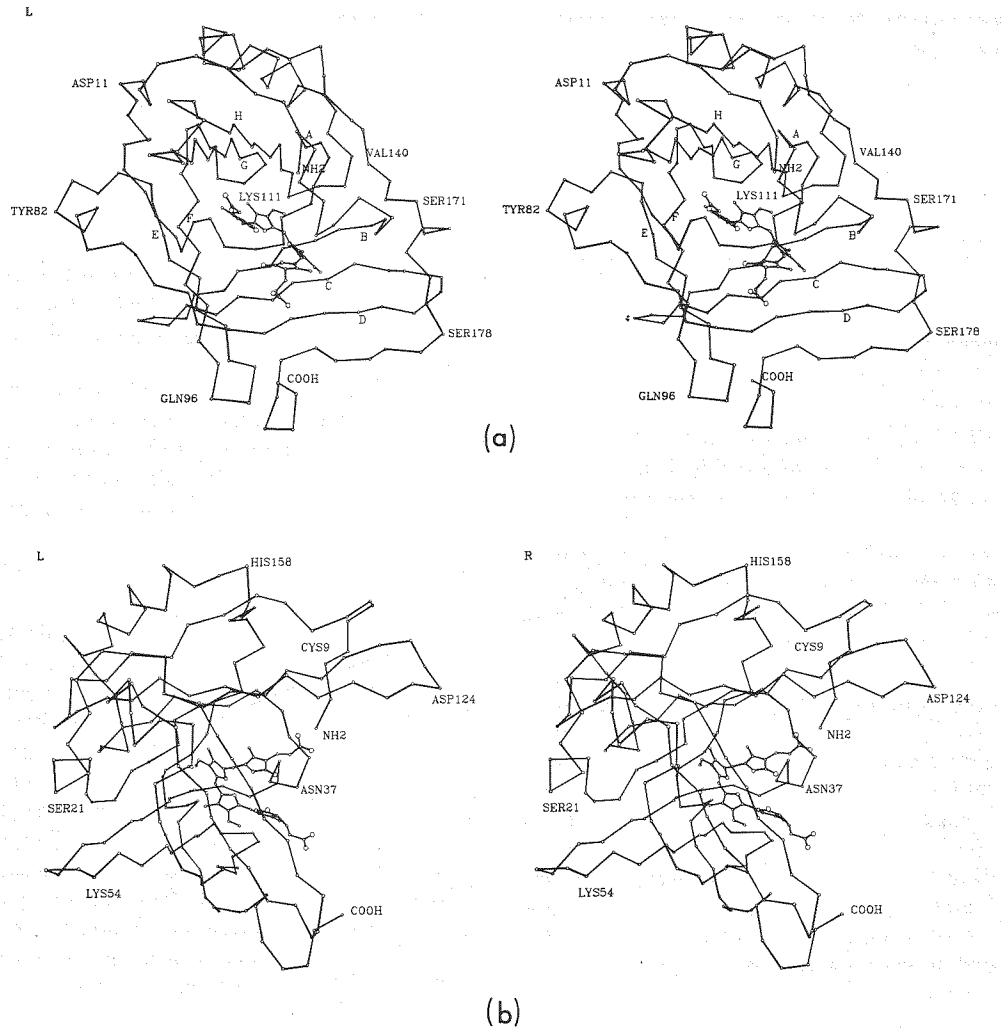


**Fig. 2.** Stereo view of an $\alpha$-carbon model of an insecticyanin subunit with the bound biliverdin. **(a)** This view looks down into the $\beta$-barrel. The eight strands of the barrel are labelled A–H; the N and C termini are labelled NH2 and COOH, respectively. The positions of several amino acid residues are indicated to aid the reader in following the structure. **(b)** This view is rotated ~90° from **(a)**. Note the orthogonal packing of the $\beta$-sheets as well as the positions of the N and C termini.

surface. The two most electron-dense peaks in the map correspond to the two disulfide bridges between residues 9–119 and 43–175. Overall the electron densities attributable to the side chains are strong and well-ordered, especially for the many aromatic amino acid residues found in insecticyanin. The exceptions are several lysine and glutamate residues located at the surface of the molecule where their side chain densities are weak. The side chain density for His 122 is missing but this residue is also located at the molecular surface. Other than these disordered side chains, the amino acid sequence determined by Riley *et al.* (1984) is in complete agreement with our electron density maps at 2.6 Å resolution.

The main secondary structural element of an insecticyanin subunit is an eight-stranded anti-parallel $\beta$-barrel which is closed at one end but open to the solvent at the other end. There is also one major $\alpha$-helix of 16 amino acid residues. An $\alpha$-carbon model of one subunit is shown in Figure 2 where the $\beta$-strands are labelled A–H. Residues of insecticyanin which participate in $\beta$-strands, $\alpha$-helices and turns are given in Table I. The list is based on visual inspection of the model and consideration of the hydrogen bonding patterns and respectively $\phi$ and $\psi$ values. The N-terminal

**Table I.** Secondary structure pattern of insecticyanin

| Residue number | Type of secondary structure |
|---|---|
| 19–24 | $\alpha$-helix |
| 30–33 (A) | $\beta$-sheet |
| 36–39 | $\alpha$-helix |
| 43–50 (B) | $\beta$-sheet |
| 51–54 | reverse turn |
| 55–62 (C) | $\beta$-sheet |
| 63–66 | reverse turn |
| 67–72 (D) | $\beta$-sheet |
| 77–83 | $\alpha$-helix |
| 86–93 (E) | $\beta$-sheet |
| 94–97 | reverse turn |
| 98–110 (F) | $\beta$-sheet |
| 111–113 | reverse turn |
| 114–122 (G) | $\beta$-sheet |
| 123–126 | reverse turn |
| 127–136 (H) | $\beta$-sheet |
| 142–157 | $\alpha$-helix |
| 172–175 | $\alpha$-helix |

glycine sits near the opening to the chromophore-binding pocket, and the first 1−18 residues form a loop which wraps around the β-barrel. Likewise, residues 158−189 form another loop wrapping around the opposite side of the barrel with the C terminus also sitting near the opening of the binding pocket. The N- and C-terminal residues are separated by ~20 Å. Both disulfide bridges are located near the surface of the molecule and are ~30 Å apart. The disulfide bridge between residues 9 and 119 links β-strand G with the N-terminal region and is located near the opening of the binding pocket. The bridge created by residues 43−175 is located on the opposite side of the pocket opening and connects the C-terminal loop with β-strand B. There are five reverse turns that connect β-strands B−C, C−D, E−F, F−G and G−H. β-Strands A and B and D and E are connected by short helical turns.

The electron density corresponding to the biliverdin is shown in Figure 3. As can be seen the chromophore binds in a closed conformation with its two propionate side chains facing the solvent. The carboxylate group of one of the propionates forms a salt bridge with the guanidium group of Arg 97 while the other carboxylate group is within hydrogen-bonding distance to the $NH_2$ group of Asn 118. The small peak of electron density which appears to be coordinated by the nitrogens of the pyrrole rings is most likely a solvent molecule or some type of ion. As expected, the binding pocket is decidedly hydrophobic. The four pyrrole rings of the biliverdin form hydrophobic interactions with Leu 35, Leu 101, Phe 61, Trp 133 and Met 70. A close-up view of the biliverdin-binding site is shown in Figure 4 and, as can be seen, Phe 61, Trp 133 and Met 70, in fact, form stacking interactions with these pyrrole rings. Other aromatic residues near the chromophore include Phe 92, Phe 94, Tyr 48 and Tyr 88.

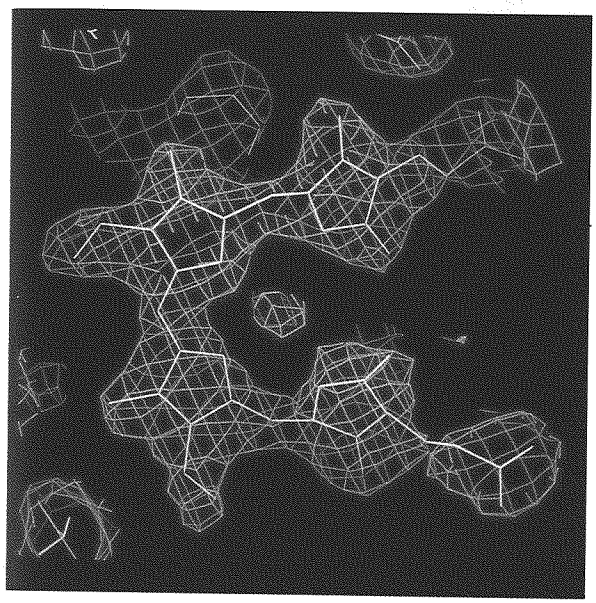

**Fig. 3.** Electron density corresponding to the biliverdin chromophore. As can be seen, the electron density attributable to the chromophore is well-ordered and shows it to be the γ-isomer of biliverdin. The small peak of electron density in the middle of the photograph is most likely a bound solvent molecule or ion.

The two subunits of insecticyanin in the asymmetric unit are related by a 'local' 2-fold rotation axis. The crystalline packing is such, however, that these subunits lie in a 222 tetrameric arrangement with one of the molecular axes coincident to the [110] crystallographic dyad. Figure 5a,b,c shows the molecular interactions between the various subunits viewed down the three symmetric axes. The individual subunits are labelled I, II, III and IV. For clarity, only two subunits are shown for each view; subunit I and the subunit related to it by the respective symmetry axis. As can be seen in Figure 5, the molecular interactions along the crystallographic dyad are clearly the most extensive with molecular contacts primarily made through amino acid residues 8−16 and 76−85 (subunits I and IV). Residues 76−85 are in an α-helical conformation with Tyr 82 of subunit I pointing into the binding pocket of subunit IV. Monomer:monomer contacts between subunits I and II are made through symmetry-related residues 143−156 which form the major α-helix (Figure 5b). There are very few contacts between subunits I and III. Details concerning the tetrameric contacts will be described more fully when the insecticyanin structure has been refined.

## Discussion

When we began our X-ray crystallographic investigation of insecticyanin, the structures of two biliproteins, namely the C-phycocyanins from *Mastigocladus laminosus* and *Agmenellum quadruplicatum*, were known (Schirmer *et al.*, 1985, 1986). Since the C-phycocyanin structures were predominantly helical it was assumed at the time that insecticyanin might also have the same helical type structure. Even at low resolution, however,

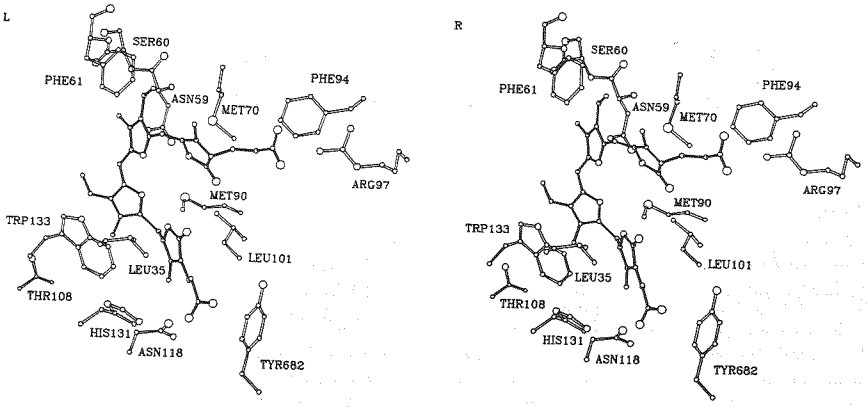


**Fig. 4.** Stereo view of the chromophore in the binding pocket. The amino acid residues shown here are within 3.5 Å of the biliverdin. Residues Phe 61, Trp 133 and Met 70 form stacking interactions with the pyrrole rings of the chromophore. The tyrosine residue labelled 682 in the drawing belongs to a symmetry-related subunit.

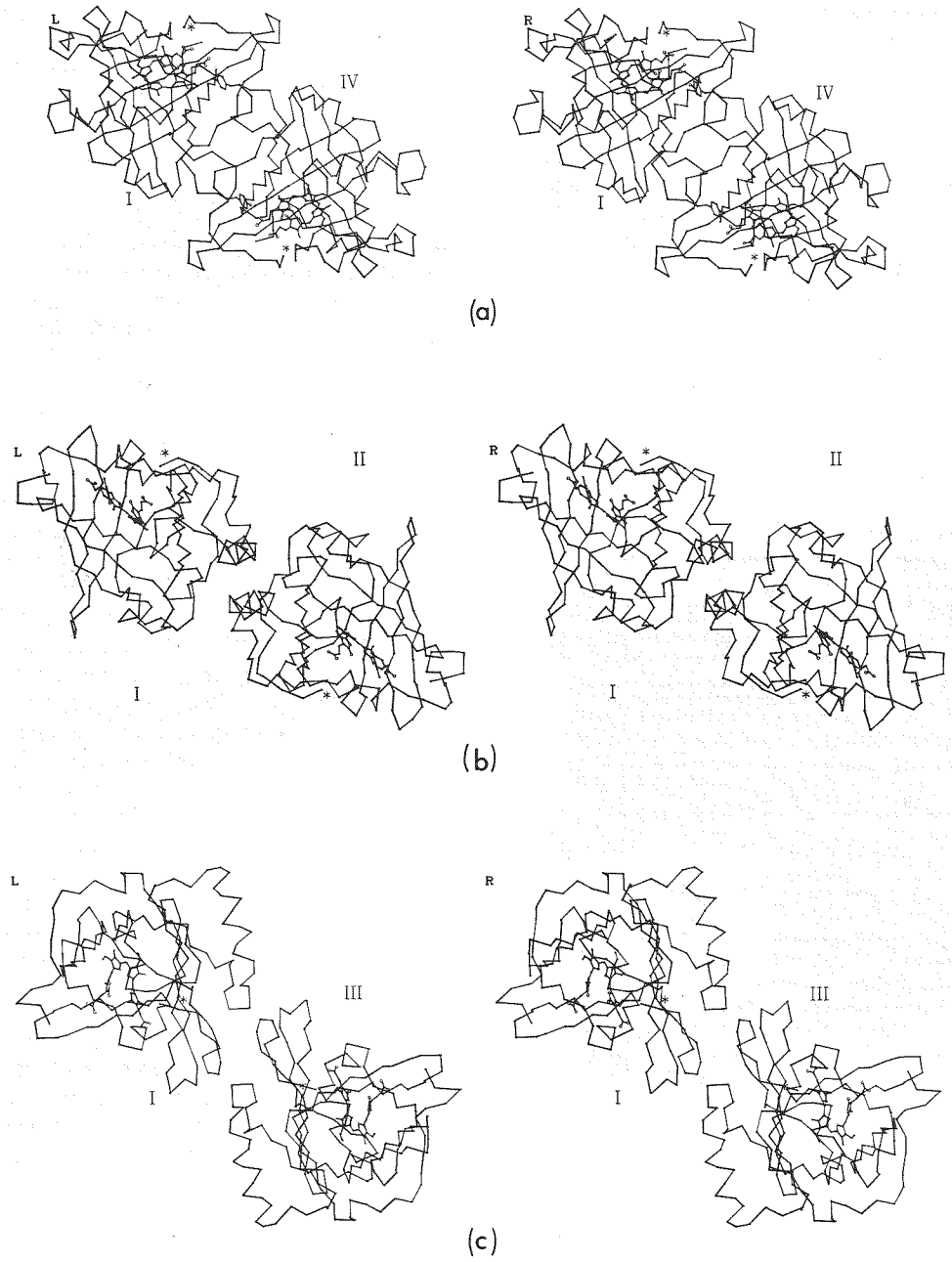


**Fig. 5.** Stereo view of the molecular interactions along the three 2-fold axes of the tetramer. The subunits are labelled I–IV. For clarity only two of the subunits, related by the respective symmetry axis, are shown in each view. The N-terminal region of each subunit is indicated by an asterisk. **(a)** Viewed down the [110] crystallographic dyad. Note that Tyr 82 of subunit I forms part of the binding pocket of subunit IV and vice versa. **(b)** Viewed down the local 2-fold axis which is inclined at an angle of 3° with respect to the *c*-axis. This dyad was used in the molecular averaging process. **(c)** Viewed down the local 2-fold axis, 90° from **(a)** and **(b)**.

it was clear that insecticyanin was a tetramer and that the individual subunits were composed primarily of $\beta$-pleated sheet.

The high resolution molecular model of insecticyanin presented in this report was built without any preconceived idea of its three-dimensional fold. As the chain tracing progressed it became apparent, however, that insecticyanin resembled closely both $\beta$-lactoglobulin (Papiz *et al.*, 1986) and the human serum retinol-binding protein (Newcomer *et al.*, 1984). All three proteins contain the same structural motif; an eight-stranded $\beta$-barrel flanked on one side by an $\alpha$-helix. A detailed comparison of these three proteins will be made once the coordinate refinement of insecticyanin, which is in progress, has been completed.

The conformation of the chromophore was also unanticipated. From the reported structures of the bilins in the phycocyanins-C, we expected the biliverdin to be in an extended conformation. In contrast, the chromophore adopts a compact configuration, much like a heme. This suggests that perhaps apo-insecticyanin first binds heme, which is then oxidized to biliverdin IX$\gamma$ while the chromophore is held in place by the protein. Our study unambiguously confirms that the chromophore is the $\gamma$-isomer of biliverdin as was first suggested by the t.l.c. experiments of Cherbas (1972) and the proton n.m.r. spectroscopic measurement of Goodman *et al.* (1985).

In retrospect, the similarity between insecticyanin and the retinol-binding protein may not be surprising since both bind highly conjugated and hydrophobic ligands. Indeed, the structural

motif found in insecticyanin, the retinol-binding protein and β-lactoglobulin may be present in other proteins, such as the fatty acid-binding proteins, whose biological role is to transport hydrophobic ligands. Furthermore, the structural relationship between insecticyanin and the retinol-binding protein suggests that the ligand binding specificity of apo-insecticyanin may be quite broad and experiments to test this hypothesis are in progress.

## Materials and methods

*Biochemical methods*

The purification of insecticyanin from *M. sexta* L. was routinely carried out by the method of Riley *et al.* (1984). Crystals of insecticyanin were grown in small glass test tubes at room temperature. Typically for these micro-batch experiments, 50 μl of protein solution were mixed vigorously with 50 μl of 40% w/v polyethylene glycol 8000 at 4°C. The initial protein concentration was at 5 mg/ml in 10 mM succinate, 0.1 mM sodium azide, pH 5.5 and the polyethylene glycol solution contained 200 mM NaCl, 200 mM succinate, pH 5.5. The test tubes were then placed in a Styrofoam box and allowed to warm slowly to room temperature. Crystallization was generally complete within 4–6 weeks. The crystals belong to the tetragonal space group $P4_32_12$ with unit cell dimensions of $a = b = 115.36$ Å, $c = 71.49$ Å and contain two subunits per asymmetric unit (Holden *et al.*, 1986). The solvent content is ~54%.

Initial heavy atom derivative searches were conducted at pH 5.5. All attempts to prepare derivatives at this pH failed. However, it was found that native crystals could be transferred to a synthetic mother liquid buffered at pH 7.5 with 50 mM $Na^+/K^+$ phosphate with no apparent deterioration of their diffraction pattern or of their physical morphology. At this pH three heavy atom derivatives were readily prepared using 10 mM $(CH_3)_3PbOOCH_3$, 5 mM *p*-hydroxymercuriphenyl sulfonic acid (PHMBS) and 5.0 mM $K_2PtCl_6$.

*X-ray data collection and processing*

X-ray diffraction data were collected from the native crystals and from the native–heavy atom complexes by the method of oscillation photography. The X-ray source was nickel-filtered copper Kα radiation from an Elliot GX20 rotating anode operated at 35 kV and 35 mA. An oscillation angle of 1.5° per film pack was used and the crystal was rotated about the *c*-axis through a net rotation of 45°. The typical exposure time was either 6 or 8 h per film pack with a crystal-to-film distance of 80 mm. By making an appropriate translation only two crystals were required for each data set.

During the initial stages of data collection it was found that the crystals had a tendency to slip in the capillary tubes. In order to prevent such problematic slippage, the insecticyanin crystals were first mounted in quartz capillary tubes, the excess mother liquid removed and then a small volume of a 0.2% solution of poly(vinyl formal) in 1,2-dichloroethane was drawn over the crystal to form a very thin plastic film. The excess poly(vinyl formal) solution was then removed with thin paper swabs and the film allowed to dry for a few minutes. The capillary tube was then sealed in the normal manner. This method, previously described for the southern bean mosaic virus Type II crystals (Rayment *et al.*, 1977), worked exceedingly well with insecticyanin.

The X-ray films were digitized with an Optronics film scanner and subsequently processed using a set of programs originally developed by Dr Michael Rossmann at Purdue University and modified by Dr Brian Matthew's laboratory at the University of Oregon (Schmid *et al.*, 1981). The films were integrated to 2.6 Å resolution. Derivative data sets were scaled to the native data in shells of equal volume in reciprocal space based on $(\sin\theta/\lambda)^2$. To take into account the extra scattering by heavy atoms, scale factors were calculated for each derivative by the method of Kraut *et al.* (1962). Relevant data collection statistics may be found in Table II.

*Computational methods*

The positions of the heavy atom binding sites were determined by inspection of the respective difference Patterson maps and placed on a common origin by use of appropriate difference Fourier maps. The program HEAVY (Terwilliger and Eisenberg, 1983) was then used to refine the positions and occupancies of the heavy atom sites as presented in Table III. Protein phases were calculated by the method of multiple isomorphous replacement (MIR). Relevant phase calculation statistics are given in Table IV.

The initial electron density maps were calculated to 5.0 Å resolution using centroid protein phases and a structure factor weighting scheme based on the figure of merit. From these maps, plotted on transparencies, the molecular boundaries were immediately obvious. Also, these maps showed that the two subunits within the asymmetric unit were related by a non-crystallographic 2-fold rotation axis tilted by several degrees with respect to the *c*-axis. The position of this local dyad was refined by a search procedure which minimized the difference in electron density between 2-fold related points in the protein map. It was found to be tilted at 3.0° with respect to the *c*-axis and intersecting the crystallographic dyad the fractional coordinates: $x = 0.6718$, $y = 0.6718$, $z = 0.0000$.

Once the position of the local dyad was refined, an electron density map was calculated to 3.0 Å resolution and globally averaged about this symmetry axis according to the method of Bricogne (1976). The molecular boundaries were then extracted from this averaged map. The electron density enclosed within the envelope accounted for 63% of the total density in the map. Using the resulting molecular envelope, 30 cycles of averaging and solvent flattening were applied at 3.0 Å resolution in order to improve the quality of the protein phases. It was decided to average the electron density map to 3.0 Å initially because, as can be seen from Table IV, the quality of the MIR protein phases drops off significantly at higher resolution. The structure factor weighting algorithm used in the aver-

**Table II.** Intensity statistics for the native and derivative crystals

| | Native | $(CH_3)_3PbOOCH_3$ | PHMBS | $K_2PtCl_6$ |
|---|---|---|---|---|
| Number of film packs | 33 | 31 | 31 | 32 |
| Average $R_{sym}$[a] (%) | 2.8 | 3.6 | 3.7 | 3.8 |
| Average $R_{sca}$[a] (%) | 3.5 | 2.9 | 2.7 | 3.1 |
| $R_{merge}$[a] (%) | 6.5 | 7.3 | 6.2 | 6.5 |
| Total reflections measured | 44 614 | 40 795 | 46 651 | 47 086 |
| Independent reflections | 14 167 | 13 522 | 13 779 | 13 834 |
| Resolution (Å) | 2.6 | 2.6 | 2.6 | 2.6 |
| Average isomorphous differences[b] (%) | – | 13.6 | 18.7 | 9.0 |
| Cell dimensions | | | | |
| *a,b* (Å) | 115.36 | 115.36 | 115.50 | 115.42 |
| *c* (Å) | 71.49 | 71.47 | 71.27 | 71.39 |

[a] $R = \Sigma|I - \bar{I}|/\Sigma I$. $R_{sym}$ measures the agreement between symmetry-related reflections on the same film, $R_{sca}$ measures the agreement between reflections recorded on successive films in a given film pack and $R_{merge}$ gives the overall agreement between intensities measured on different films. [b] $R = \Sigma||F_N| - |F_H||/\Sigma|F_N|$ where $|F_N|$ is the native structure factor amplitude and $|F_H|$ is the derivative structure factor amplitude.

**Table III.** Refined heavy atom parameters[a]

| Derivative | Site no. | Relative occupancy | *x* | *y* | *z* | B | Location |
|---|---|---|---|---|---|---|---|
| $(CH_3)_3PbOOCH_3$ | 1 | 0.2722 | 0.8742 | 0.8042 | 0.9856 | 33.52 | Glu 68 |
| | 2 | 0.2687 | 0.6397 | 0.9788 | 0.6935 | 33.77 | |
| $K_2PtCl_6$ | 1 | 0.0837 | 0.9508 | 0.8525 | 0.7185 | 34.18 | Asp 124 |
| | 2 | 0.1390 | 0.8880 | 0.7032 | 0.5591 | 30.02 | |
| PHMBS | 1 | 0.3642 | 0.5145 | 0.8741 | 0.7960 | 21.19 | His 189 |
| | 2 | 0.2530 | 0.8525 | 0.7673 | 0.8216 | 32.35 | |

[a] *x*, *y*, *z* are the fractional atomic coordinates, B is the thermal factor in $A^2$.

**Table IV.** Phase calculation statistics

| | Resolution range | | | |
|---|---|---|---|---|
| | Infinity to 10.0 Å | 5.0 Å | 3.3 Å | 2.6 Å |
| No. of reflections | 301 | 1942 | 4939 | 6985 |
| Figure of merit | 0.75 | 0.73 | 0.54 | 0.53 |
| Phasing power $[(CH_3)_3PbOOCH_3]$ | 1.56 | 1.76 | 1.14 | 1.05 |
| Phasing power ($K_2PtCl_6$) | 0.86 | 0.96 | 0.56 | 0.46 |
| Phasing power (PHMBS) | 1.44 | 1.48 | 1.03 | 1.15 |

Phasing power is the ratio of the root mean square heavy atom scattering factor amplitude to the root mean square lack of closure error.

aging process was of the form $w = e-(|F_o| - |F_c|)/|F_o|$ where $|F_o|$ was the observed structure factor amplitude and $|F_c|$ was the calculated structure factor amplitude (Rayment, 1983). After 30 cycles of refinement the overall R factor between the observed and calculated structure factors was 14.1%. This R factor was calculated as $\Sigma||F_o| - |F_c||/\Sigma|F_o|$ where $|F_o|$ was the observed structure factor amplitude and $|F_c|$ was the calculated structure factor amplitude. The R factor as a function of resolution was uniformly level except for the shell of data between 3.2 and 3.5 Å resolution. The high R value of 23.3% in this resolution range was a consequence of series termination errors (Rayment,1983).

The molecular averaging from 3.0 Å to 2.6 Å resolution was carried out in increments of 0.1 Å. Phases from the 3.0 Å resolution averaging procedure were combined with the MIR phases between 3.0 Å and 2.9 Å resolution and 30 cycles of molecular averaging and solvent flattening applied. These 'refined' 2.9 Å phases were then combined with MIR phases from 2.9 Å and 2.8 Å and the averaging/solvent flattening process repeated for another 30 cycles. This cycling procedure was continued out to 2.6 Å resolution. The final overall R factor after averaging was 13.7% for 14 167 reflections. Again the distribution of R values as a function of resolution was very level, gradually rising from 10% at 5 Å resolution to 20% at 2.6 Å resolution. The root mean square phase change between the next to the last and the last cycle of averaging was 1.16°.

It is important to note that the electron density outside the molecular envelope was set to its averaged value rather than to numerical zero as is frequently done. In addition, no constraints were made on the electron density within the envelope except for that imposed by the local 2-fold axis. Attempts to truncate the negative electron density within the molecular boundaries by a variety of attenuation algorithms led to protein maps of rather poor quality where the polypeptide chain was broken and ambiguous in numerous places. In maps where the negative electron density had not been artificially truncated the course of the polypeptide chain was immediately obvious and was readily traced on minimaps plotted on stacked plastic sheets.

An ideal molecular model was fitted to the averaged electron density map on an Evans and Sutherland PS330 graphics system using the program FRODO (Jones, 1985). The fitting process took ~60 h and all of the electron density has been accounted for in the chain tracing.

## Acknowledgements

This work has benefited from the helpful discussions of Drs Larry Weaver, Ted Baker, John Kawooya and Robert Ryan. We would also like to thank Dr Brian Matthews for allowing us to use his film scanner and Dr Terry Meyer for suggesting the three-dimensional similarity between insecticyanin and the retinol-binding protein. Initial heavy atom derivative searches were conducted by Ralph Martel whose help is gratefully acknowledged. This research was supported by grants to I.R. (AM GM 351865 and BRSG 829023) and to J.H.L. (NIH GM 29238). I.R. is an established investigator of the American Heart Association.

## References

Bricogne,G. (1976) *Acta Crystallogr.*, **A32**, 832–837.
Cherbas,P.K. (1973) Ph.D. Thesis, Harvard University.
Goodman,W.G., Adams,B. and Trost,J.T. (1985) *Biochemistry*, **24**, 1168–1175.
Holden,H.K., Law,J.H. and Rayment,I. (1986) *J. Biol. Chem.*, **261**, 4217–4218.
Jones,T.A. (1985) *Methods Enzymol.*, **115**, 157–171.
Kawooya,J.K., Keim,P.S., Law,J.H., Riley,C.T., Ryan,R.O. and Shapiro,J.P. (1985) *ACS Symp. Ser.*, **276**, 511–521.
Kraut,J., Sieker,L.C., High,D.F. and Freer,S.T. (1962) *Proc. Natl. Acad. Sci. USA*, **48**, 1417–1424.
Newcomer,M.E., Jones,T.A., Åqvist,J., Sundelin,J., Eriksson,U., Rask,L. and Peterson,P.A. (1984) *EMBO J.*, **3**, 1451–1454.
Papiz,M.Z., Sawyer,L., Eliopoulos,E.E., North,A.C.T., Findlay,J.B.C., Sivaprasadarao,R., Jones,T.A., Newcomer,M.E. and Kraulis,P.J. (1986) *Nature*, **324**, 383–385.
Rayment,I. (1983) *Acta Crystallogr.*, **A39**, 102–116.
Rayment,I., Johnson,J.E. and Suck,D. (1977) *J. Appl. Crystallogr.*, **10**, 365.
Riddiford,L.M. (1982) *Dev. Biol.*, **92**, 330–342.
Riley,C.T., Barbeau,B.K., Keim,P.S., Kezdy,F.J., Heinrikson,R.L. and Law, J.H. (1984) *J. Biol. Chem.*, **259**, 13159–13165.
Schirmer,T., Bode,W., Huber,R., Sidler,W. and Zuber,H. (1985) *J. Mol. Biol.*, **184**, 257–277.
Schirmer,T., Huber,R., Schneider,M., Bode,W., Miller,M. and Hackert,M.L. (1986) *J. Mol. Biol.*, **188**, 651–676.
Schmid,M.F., Weaver,L.H., Holmes,M.A., Grutter,M.G., Ohlendorf,D.H., Reynolds,R.A., Remington,S.J. and Matthews,B.W. (1981) *Acta Crystallogr.*, **A37**, 701–710.
Terwilliger,T.C. and Eisenberg,D. (1983) *Acta Crystallogr.*, **39A**, 813–817.

*Received on March 10, 1987*